Cyclic Behavior of Extruded Magnesium

Clervie Guillemer [a], Michel Clavel [b], Georges Cailletaud [c]

[a] LTI, UPJV, Amiens, France
[b] MSSMAT, École Centrale de Paris, France
[c] École des Mines de Paris, Centre des Matériaux, Évry, France.

Abstract
The mechanical cyclic behavior of extruded magnesium is strongly anisotropic, mainly due to crystallographic texture generated by the extrusion process. The purpose of the present study is to better understand the cyclic behavior of such a metal submitted to small cyclic symmetric plastic strains ($\Delta\varepsilon p/2 = \pm.1\%$ and $\pm.4\%$). Deformation mechanisms (slip and twin systems) have been observed by TEM. Based on microscopic observations, a crystal-plasticity-based constitutive model has been developed. It is shown that basal slip is very easy to activate even for small Schmid factors. The asymmetry between tensile and compressive loadings mainly results from the activation of hard slip systems in tension (such as <a> pyramidal and prismatic and <c+a> pyramidal glides) and twinning in compression. Numerical simulations reveal that untwining in tension subsequent to compression must be considered to correctly fit the experimental hysteresis curves.

1 INTRODUCTION

Magnesium alloys are increasingly used for lightweight structural components in automotive industry. Vibrations in moving vehicle lead to cyclic loading of the components and necessitate focusing on fatigue behavior of magnesium alloys. Although cast alloys are more generally used, cast defects tend to limit ductility. Wrought alloys offer better mechanical properties but the strong crystallographic texture inherited from the deformation process leads to strong anisotropic properties. More particularly in terms of cyclic loading, hysteresis loops are asymmetric under strain-controlled tests [1-4] and compressive ratcheting is observed under symmetric stress-controlled tests [5].
To accommodate deformation at room temperature in the hexagonal close packed (HCP) magnesium and Mg alloys, basal slip, i.e. slip on the (0001) plane with <11-20> Burgers vector, prismatic (10-10) <11-20> and pyramidal (10-11) <11-20> slips may be activated. The critical resolved shear stress (CRSS) of basal slip is very low (around 1MPa), prismatic and pyramidal slips exhibit CRSS about 50 times larger. Since the <11-20> slip direction is perpendicular to the c-axis, glide on previously listed systems cannot produce any deformation along the c-axis. To accommodate straining in the c-direction, deformation mechanisms with <c> or <c+a> directions must be operative. <c+a> i.e. <11-23> slips on first-order (10-11) and second order (11-22) pyramidal planes are sometimes reported [6, Agnew1] but (10-12) <10-1-1> twinning is believed the dominant mechanism at room temperature [8, 9] due to quite low CRSS. Due to the "polar" nature of twinning [10], the activation of the (10-12) twinning is associated with a contraction parallel to the c direction and with an extension in a direction lying in the basal plane in HCP materials such as magnesium.

2 MATERIAL AND EXPERIMENTAL PROCEDURE

The material used in this work is a commercially pure magnesium, that was hot rolled, hot extruded and finally recristallized. The microstructure consists of equiaxed grains of about 60 µm. Rolling or extrusion operations generate a strong basal texture with the c-axis lying normal to the sheet. As expected, a high concentration of basal directions is observed perpendicular to extrusion axis. It is worth noting that the texture is not axisymetric, see Figure 1a, probably due to extrusion subsequent to rolling. Figure1b shows the recalculated pole figures that will be used in the modeling, on a section perpendicular to the extrusion axis.
Cyclic cylindrical specimens with a 5 mm diameter and a 12 mm gauge length were taken from the rod in the direction of extrusion. The stress-strain characteristics of the material were obtained using a Mayes ESHF50 load frame equipped with a 50kN load cell. The strain was measured using a ± 10% Instron extensometer with a gauge length of 10 mm. Tensile and compressive tests were performed at a 10^{-4} Hz strain rate when the cyclic specimens were strained at a 10^{-3} Hz strain rate. Cyclic tests were conducted under constant applied plastic strain amplitude $\Delta\varepsilon p/2$ for a better cycle to cycle reproducibility. All cyclic tests start in tension.

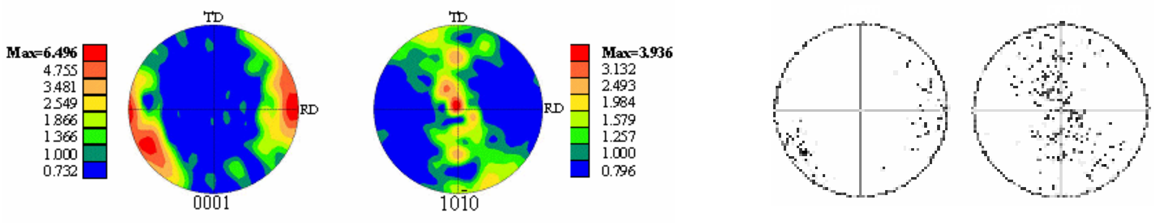

Figures 1. a) Experimental pole figures obtained by Electron Back Scattering Diffraction (EBSD). The center of the projection is parallel to the extrusion axis. b) Recalculated pole figures (343 grains)

Thin foils were prepared for TEM by cutting thin slices from within the gauge lengths of selected specimens, mechanically ground to a thickness of about 150 µm and electrolytically polished to perforation using a solution of 10 vol.% perchloric acid-90 vol.% acetic acid at 15°C with an applied voltage of 20V. Prior observations the specimens were immersed in a 5 vol.% nitric acid-95 vol.% ethanol solution (nital) during 10s in order to remove black spots on the surface of the thin foil. TEM observations were made with a Jeol 200CX microscope operating at a voltage of 120 kV. Observations under optical microscopy were made after gentle polishing and nital etching.

3 EXPERIMENTAL RESULTS

3.1 Mechanical Results

Monotonic tensile and compressive tests were conducted to a plastic deformation of .1%, Cf. Figure 2. Whatever the loading direction, the Young modulus is about 40 GPa and the yield stress is 6 MPa. Consistent with reports in literature [2,3,8,11], a large asymmetry of hardening evolution is evidenced in tensile and compressive tests. A high strengthening rate develops in compression just after yielding, following by a saturation of the stress for plastic strains higher than .01%. During tensile loading, the strengthening rate is high and evolves linearly with plastic strain.

Cyclic tests were conducted under symmetric constant applied plastic strain amplitudes $\Delta\varepsilon p/2$ = .1% and .4% until fracture. Figure 3 and Table I indicate that the hysteresis loops are strongly asymmetric, since the hardening is important in positive loading whereas it is quite nil in compression as noticed for monotonous loadings. Then the compressive stress tends to reach a plateau (about 60 MPa) whatever the applied plastic strain. Reverse loading after compression leads to inflected tension portion and convex loop.

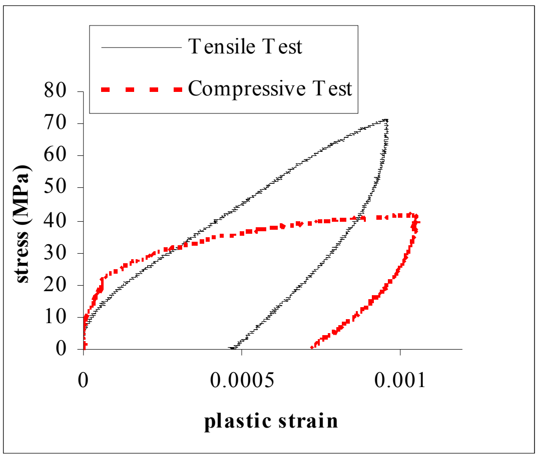

Figure 2. Monotonic tensile and compressive tests - Stress (MPa) versus plastic strain

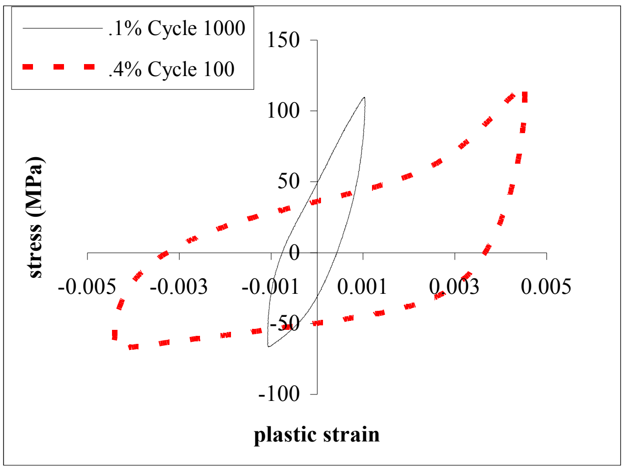

Figure 3. Cyclic tests $\Delta\varepsilon_p/2$ = .1% and $\Delta\varepsilon_p/2$ = .4% - Hysteresis loops at saturation

3.2 Optical and TEM observations :

<u>Twin surface fraction :</u> the surface fraction of twins after loading was determined by optic microscopy and image analysis on a piece cut from specimens perpendicularly to the loading axis. After one quarter of cycle of the $\Delta\varepsilon p/2$ = .1% test (i.e. tensile loading), the twin fraction equals .8% and reaches 7% after cycling at failure

(cumulated plastic strain p = 4 (Δεp/2) N = 8 with N the cycle number). Twin fraction has not been determined in compression but according to [4], it could reach around 1.4% and 5.7% for a .1% and .4% compressive plastic strains respectively. Cycling develops twin activity since the twin fraction reaches about 25% for the Δεp/2 = .4% test at failure (p = 8).

<u>TEM observations :</u>

Schmid factors are available using systematic stereographic projection and a careful orientation of the thin foil respective to loading axis. After .1% tensile strain, deformation characteristics have been observed using TEM in 3 neighboring grains i.e. at a triple boundary, Cf. Figures 4. According to the crystallographic orientation, grains exhibit either twin or <a> and <c+a> pyramidal slips (Schmid factors are respectively .33 and .49) or <a> prismatic slip (Schmid factor equals .35). Due to the crystallography of twinning, no twin is expected in tension. Twinning in grain 1 may be due to large back stresses due to misorientation between neighboring grains. The <c+a> first-order slip system in the second grain is activated under high Schmid factor and it is usually observed in the grain boundary region, as a consequence of strain incompatibilities. Other observations indicate basal slip under very low Schmid factors of about .17. A .1% compressive strain activates especially (10-12) <1101>-type twinning and basal slip.

After a Δεp/2 = .1% cyclic loading, (10-12) <1101>-type twinning and <a> basal, prismatic and pyramidal slips are observed as well as <c+a> pyramidal slip which is more particularly confined near grain or twin boundaries. Deformation in twins is obvious, even if it is not possible to determine the nature of such deformation: twinning or slip. A Δεp/2 = .4% cyclic loading makes the dislocation density more important and intensive slip in twins is activated, Cf. Figures 5. Whatever the test, complex dislocation structures were never found which could support a very weak occurrence of cross slip. As a remark, no <c+a> slip on second-order (11-22) pyramidal plan is observed.

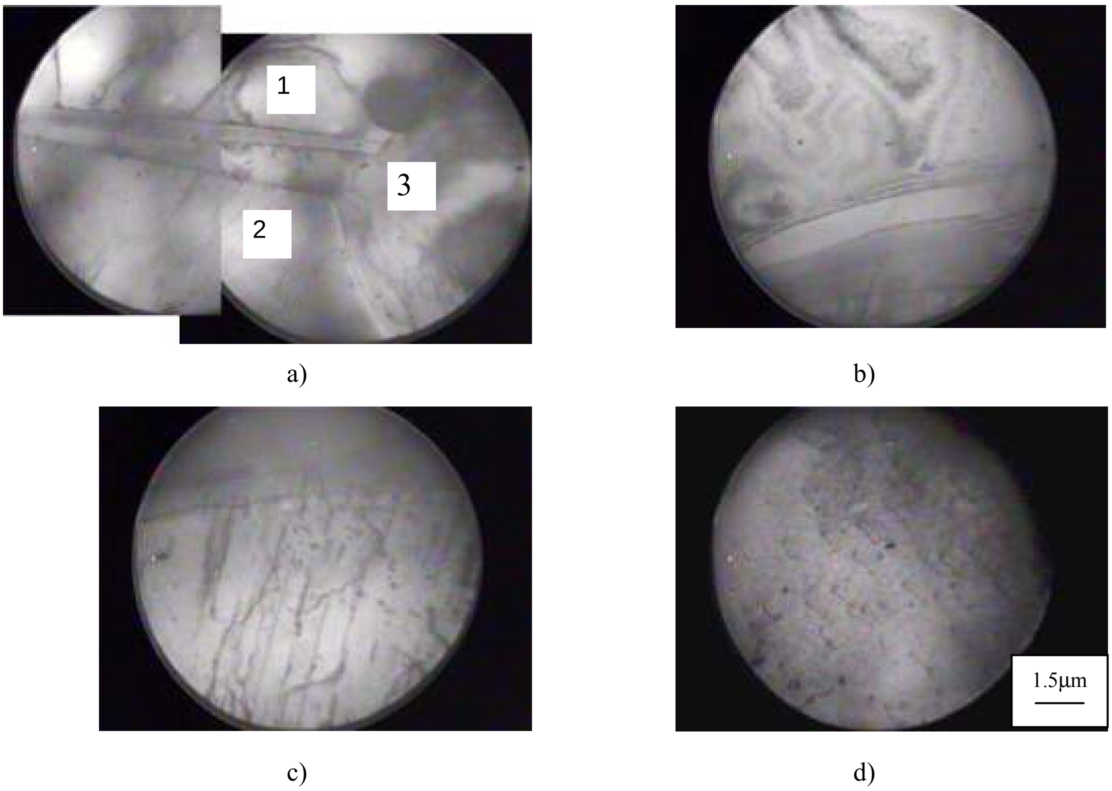

Figures 4. TEM observations – Tensile test $\varepsilon^p = 0.1\%$ – a) Grains location at a triple boundary, b) Twin in grain 1, c) <a> and <c+a> pyramidal glide in grain 2 (in the very vicinity of the grain boundary), d) <a> prismatic glide in grain 3

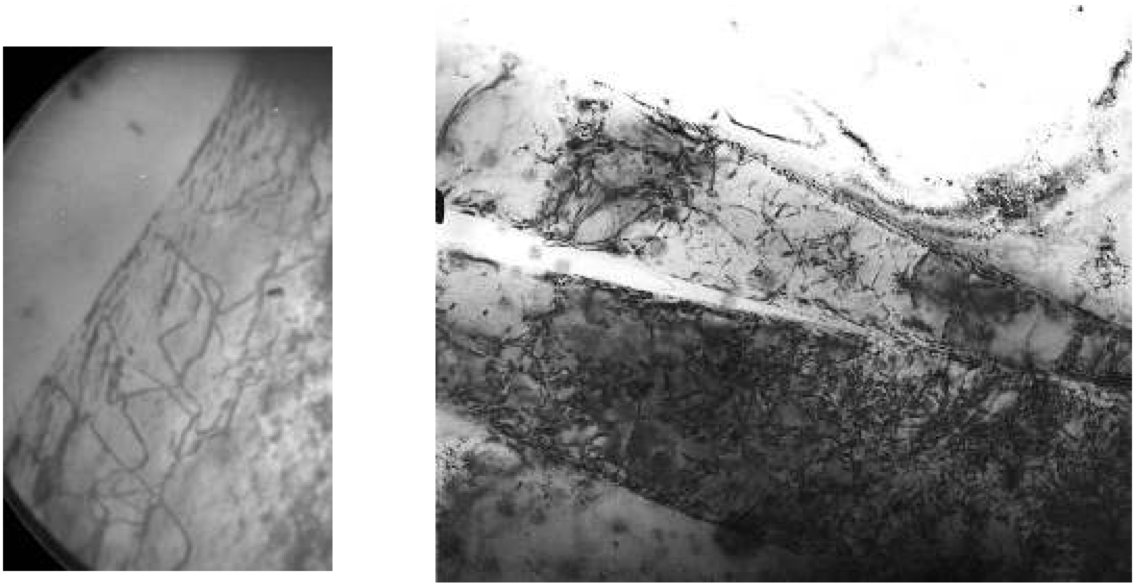

a) b)

Figures 5. TEM observations – Cyclic test $\Delta\varepsilon^p/2$ = 0.4% at fracture – a) Pyramidal <c+a> dislocations at matrix/twin interface, b) Intense slip activity inside twins

Table I. Summary of the mechanical tests: maximal positive and negative stresses Σ+ et Σ- (reached at saturation for cyclic tests); asymmetry ratio Σ+/Σ-; Optical and TEM observations.

Tests	Σ+	Σ-	Σ+/Σ-	Twin fraction	TEM observations
Tension (εp = .1%)	80			.8%	Slip (basal <a>, prismatic <a>, pyramidal <a>, pyramidal <c+a>) – (10-12) twinning
Compression (εp = .1%)		40		1.4% [4]	Slip basal <a>, (10-12) twinning
Cyclic loading (Δεp/2 = .1%)	110	67	1.64	7%	Slip and (10-12) twinning Slip or twinning in twins
Cyclic loading (Δεp/2 = .4%)	140	67	2.09	25%	Slip and (10-12) twinning Slip in twins

4 NUMERICAL MODELLING AND RESULTS

The purpose is to accurately account for the asymmetry between traction and compression and the particular shape of the hysteresis loops with the inflexion point for the test at Δεp/2 = .4%. The inputs for modeling are the experimental measured texture and TEM observation conclusions. Slips on basal, prismatic and pyramidal planes with a <11-20> Burgers vector are allowed as well as <11-23> dislocations on the first-order (10-11) plane and (10-12) <1101> twinning. The critical resolved shear stresses are reported in the following table.

Table II. CRSS used in numerical modeling for the different slip and twin systems

Slip/Twin	(0001) <11-20>	(10-10) <11-20>	(10-11) <11-20>	<11-23> (10-11)	(10-12) <10-1-1>
CRSS (MPa)	1	30	80	80	19

The experimental measured texture is discretized into a finite number (343) of grain orientations defined by three Euler angles. Such a number is representative of the material texture, see Figure 1. The multi-scale model has been implemented in the ZeBuLoN software developed by the Ecole des Mines de Paris [12].

4.1 Numerical modeling

Scale transition rules

In this study, the localization steps will be successively: the macroscopic level → grain → slip or twin system. The stress prevailing at the macroscopic scale (respectively at the grain scale) is labeled $\underline{\underline{\sigma}}$ (resp. $\underline{\underline{\sigma}}^g$). The grain is composed from twins (referred as t) and matrix (referred as 0). A "β - type law" which has been successfully developed for titanium [13] is used here to account for stress redistribution between the different scales.

$\underline{\underline{\sigma}}^g = \underline{\underline{\sigma}} + C(\underline{\underline{\beta}} - \underline{\underline{\beta}}^g)$ with $\dot{\underline{\underline{\beta}}}^g = \dot{\underline{\underline{\varepsilon}}}^g + D\underline{\underline{\beta}}^g \left\| \dot{\underline{\underline{\varepsilon}}}^g \right\|$

$\underline{\underline{\sigma}}^{gi} = \underline{\underline{\sigma}}^g + Ci(\underline{\underline{\beta}}^g - \underline{\underline{\beta}}^{gi})$ with $\dot{\underline{\underline{\beta}}}^{gi} = \dot{\underline{\underline{\varepsilon}}}^{gi} + D_i \underline{\underline{\beta}}^{gi} \left\| \dot{\underline{\underline{\varepsilon}}}^{gi} \right\|$ where i represents t or 0.

$\underline{\underline{\beta}} = \sum_g f^g \underline{\underline{\beta}}^g$ and $\underline{\underline{\beta}}^g = (1-\xi^g)\underline{\underline{\beta}}^{g0} + \sum_t \xi^{gt} \underline{\underline{\beta}}^{gt}$ with ξ^{gt}, the fraction of a twin variant in a grain and ξ^g, the total fraction of twins in a grain.

Slip mechanisms in the matrix

For each slip system ($s \in S$), the resolved shear stress is given by $\tau^s = \underline{\underline{\sigma}}^{g0} : \underline{\underline{m}}^s$ where $\underline{\underline{m}}^s$ is the Schmid tensor of the slip system. A viscoplastic model with isotropic and kinematic hardenings (respectively r^s and x^s) is used to calculate the strain rate. The parameters (K, n, b, Q, c, d) depend on the slip family. Interactions between slip systems (h_{sj}) are taken into account in the isotropic stress evolution.

$$\dot{\gamma}^s = \dot{v}^s \mathrm{signe}(\tau^s - x^s) = \left\langle \frac{\left|\tau^s - x^s\right| - r^s - \tau_y}{K} \right\rangle^n \mathrm{signe}(\tau^s - x^s)$$

$$r^s = bQ \sum_{j \in S} h_{sj} \rho^i \qquad \dot{\rho}^i = (1 - b\rho^i)\dot{v}^i$$

$$x^s = c\alpha^s \qquad \dot{\alpha}^s = \dot{\gamma}^s - d\alpha^s \dot{v}^s$$

The strain rate of the matrix due to slip mechanisms is the sum of all slip strain rates: $\dot{\underline{\underline{\varepsilon}}}^{g0} = \sum_{s \in S} \dot{\gamma}^s \underline{\underline{m}}^s$

Strain produced by twinning

Twinning formalism is close to the one developed for slip. For each twin variant (t), the shear stress is calculated from the stress prevailing at matrix scale (untwined part of the grain) $\underline{\underline{\sigma}}^{g0}$ and the Schmid tensor [8, 4]. If the resolved shear $\tau^t = \underline{\underline{\sigma}}^{g0} : \underline{\underline{m}}^t$ on a twin system is larger than a threshold, twinning develops. Twinning rate is written as a function of the plastic strain rate: $\dot{\xi}^{gt} = k(\xi_{max} - \xi^g)(\xi_{max} - \xi^{gt}) \left\| \dot{\underline{\underline{\varepsilon}}}^{g0} \right\|$

The strain in the grain due to twinning mechanisms is a weighted average of all twin variants strains: $\dot{\underline{\underline{\varepsilon}}}^{gt} = \sum_t \dot{\xi}^{gt} (\gamma_t \underline{\underline{m}}^t)$ where γ_t represents the magnitude of twinning shear and equals .131 in magnesium [10].

The plastic strain in each grain is the sum of strains due to twinning and slip in the matrix: $\dot{\underline{\underline{\varepsilon}}}^g = \dot{\underline{\underline{\varepsilon}}}^{gt} + (1-\xi^g)\dot{\underline{\underline{\varepsilon}}}^{g0}$ and the macroscopic plastic strain is written as: $\dot{\underline{\underline{\varepsilon}}}^p = \sum_g f_g \dot{\underline{\underline{\varepsilon}}}^g$ with f_g the grain fraction.

4.2 Numerical results and model revisions

Results on monotonous tests show that the model correctly takes into account the difference between tension and compression, see Figure 6. Numerical results are less than 10% far from the experimental values. On the contrary, cyclic tests are not so well captured even if the stress levels in tension and compression are still accurate. The curvature sign change of the loop after unloading for the $\Delta\varepsilon p/2 = .4\%$ cyclic test is actually not caught by the model, see Figure 7.

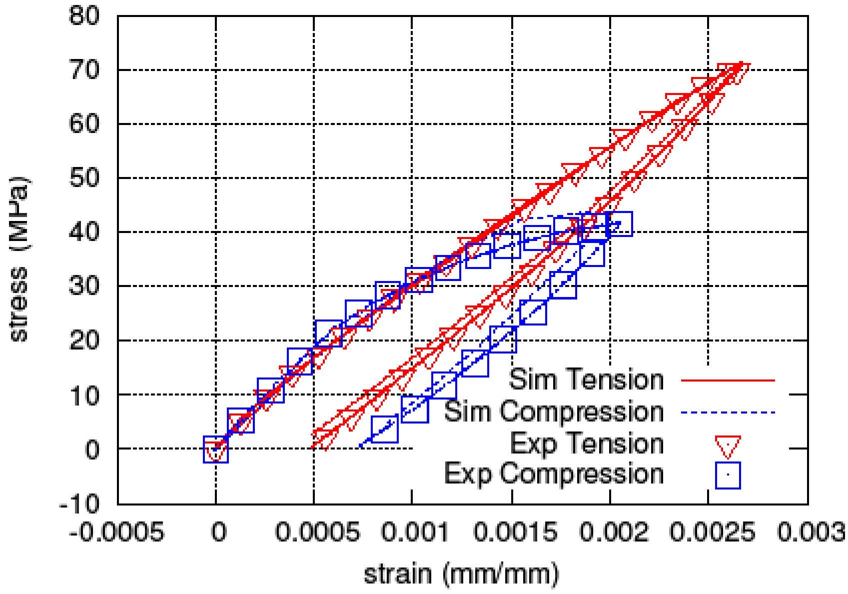

Figure 6. Modeling of monotonic tensile and compressive behavior. The model revisions do not change these results.

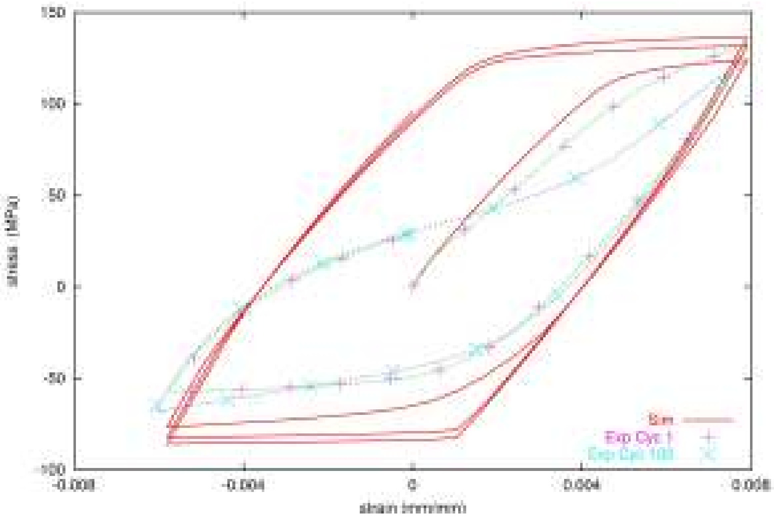

Figure 7. Modeling of cyclic behavior – $\Delta\varepsilon p/2 = .4\%$ (before revisions, without untwining)

Some recent publications all using different experimental techniques tend to evidence untwining in magnesium and magnesium alloys during reverse loading: in situ neutron diffraction [8], observations under optical microscope [4, 14], acoustic emission [4], mechanical tests [15]. Generally speaking, reversibility of the twinning process is explained by reversible movement of twin boundaries [16]. Subsequent to such observations, an untwining process is introduced in the model as follows:

$$\dot{\xi}^{gt} = -k_d \xi^{gt} \left\| \dot{\underline{\underline{\varepsilon}}} \right\|$$

The coefficient k_d differs from this one introduced in the twinning law since twin nucleation mechanisms are supposed harder than these needed for untwining (themselves harder that those needed for twin expansion [10, 4]). Moreover keeping in mind the polar nature of twinning that is favored by a contraction parallel to the c direction and an extension in a direction lying in the basal plane, a modification of twinning criterion is introduced. Due to the texture inherited from the extrusion process, the loading axis of the experimental samples is quite perpendicular to the c axis. In others words, in the present study twinning (respectively untwining) can go ahead only if a negative hydrostatic pressure (resp. positive) prevails in the grain: $\mathrm{trace}\left(\underline{\underline{\sigma}}^{g0}\right) < 0$ (resp. $\mathrm{trace}\left(\underline{\underline{\sigma}}^{g0}\right) > 0$).

Cyclic experimental and numerical results obtained after model revisions are compared in Figures 8 and 9. In particular, Figure 9 shows that untwining accounts for the particular convex curvature after unloading from compression for the Δεp/2 = .4% test. In this way, our numerical results validate the experimental observations: twins create during compressive loading tend vanish during reverse loading and all the strain caused by twinning during compressive pre-deformation is regained by untwining during tensile loading. It is worth noting that after few cycles, the modeled twin fraction tends to saturate to a value of 30% (not shown here), a very close value to the experimental one (about 25%) for the Δεp/2 = .4% test (10% instead of 7% for the Δεp/2 = .1% test).

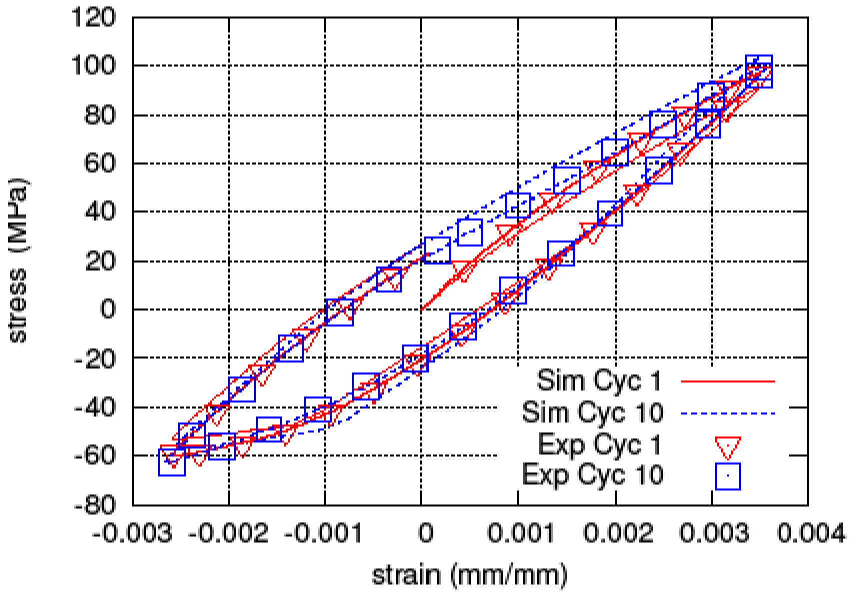

Figure 8. Modeling of cyclic behavior – Δεp/2 = .1% (after revisions, with untwining)

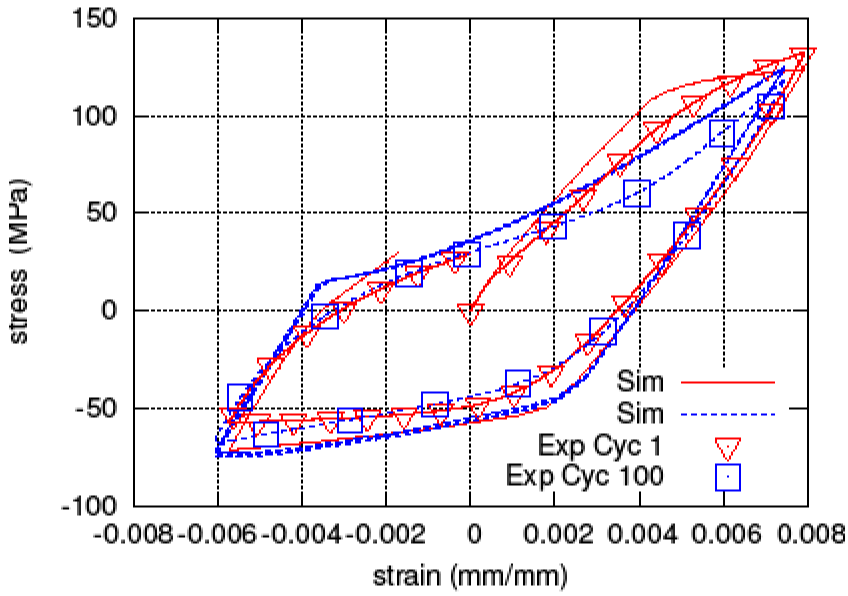

Figure 9. Modeling of cyclic behavior – Δεp/2 = .4% (after revisions, with untwining)

5 CONCLUSION

Cyclic behavior of magnesium submitted to small plastic strains ($\Delta\varepsilon p/2 = \pm.1\%$ and $\pm.4$) has been experimentally and numerically studied. Samples are loaded perpendicular to the c axis so that Schmid factors are very low for basal and prismatic slips. Nevertheless the CRSS for basal slip is so weak that this slip is activated in some grains (.17 Schmid factor) resulting in low absolute yield stress (6 MPa). The asymmetry between monotonic and compressive tests is caused by the activation of different deformation modes: hardening in tension is due to hard slip systems activation (<a> prismatic and pyramidal and <c+a> pyramidal dislocations). Twinning prevails in compression: the CRSS for twin nucleation is higher that for basal slip activation but once twinning activated, deformation proceeds under weak hardening and a kind of stress plateau is observed whatever the applied strain. The particular shape of the hysteresis curve is interpreted by untwining during tension following twinning in pre-compression. Taking into account the untwining process, numerical modeling correctly fit the experimental curves, even if the deformation observed by TEM in the twins are not considered yet.

REFERENCES

[1] Zenner H, Renner F, *Int. Journ. Plasticity*, 24, 2002, 1255-1260
[2] Nobre J.P., Noster U., Kommeier M., Dias A.M., Scholtes B., *Key Eng. Mater.*, 2002, 230-232, 267-270
[3] Noster U., Scholtes B., Z. Metallkd., 94 (5) , 2003, 559-563
[4] Lou X.Y., Li M., Boger R.K., Agnew S.R., Wagoner R.H., *Int. Journ. Plasticity*, 23, 2007, 44-86
[5] Lamark T.T., Chmelik F., Estrin Y., Lukac P., *Journ. of Alloys and Compounds*, 378 (1-2), 2004, 202-206
[6] Stohr J.F., Poirier J.P., *Phil. Mag.*, 25, 1972, 1313
[7] Agnew S.R., Horton J.A., Yoo M.H., *Metall. and Mater. Trans.*, 33A, 2002, 851-858
[8] Gharghouri MA, Weatherly GC, Embury JD, Root J., *Phil. Mag.*, 79, 1999, 1671-1695
[9] Balasubramanian S., Anand L., *Acta Mater.*, 50, 2002, 133-148
[10] Partridge P.G., *Metallurgical Reviews*, 12, 1967, 169-194,
[11] Barnett M.R., Keshavarz Z., Beer A.G., Atwell D., *Acta Mater.*, 52, 2004, 5093-5103
[12] Foerch R., Besson J., Cailletaud G., Pilvin P., *Comp. Meth. Appl. Mech. Eng.*, 141, 1997, 355-372
[13] Feaugas X., Pilvin Ph., Clavel M., *Acta Materialia*, 45 (7), 1997, 2703-2714
[14] Caceres C.H., Sumitomo T., Veidt M., *Acta Mater.*, (51), 2003, 6211-6218
[15] Kleiner S, Uggowitzer PJ, *Mater. Sci. Eng.*, 379 A (1-2), 2004, 258-263
[16] Reed-Hill RE, Dahlberg EP, Slippy Jr., *WA. AIME Trans.*, (233), 1965, 1766.